Exchange reactions in intense infrared laser fields

M. Yu. Ivanov,* D. R. Matusek, and J. S. Wright
Ottawa-Carleton Chemistry Institute, Department of Chemistry, Carleton University, Ottawa, Canada K1S 5B6
(Received 26 June 1996)

We examine the role of the dipole moment induced by an intense nonresonant infrared laser field on exchange reactions of the type $A+BC\rightarrow AB+C$. This is compared to previous work which included the effect of the permanent dipole moment and its variation along the reaction coordinate. The formalism for laser-molecule interaction is developed for the cases where the reciprocal laser frequency is comparable to or much shorter than the time required for the system to cross the transition state. It is predicted that the induced dipole moment will both lower the electronic barrier to reaction and also create bound states along the reaction path. Results of classical trajectory calculations are presented for the collinear $H+H_2\rightarrow H_2+H$ reaction, using *ab initio* dipole moment and polarizability surfaces. It is found that the collisional energy threshold for reaction is lowered significantly, and that the effects of the induced dipole moment dominate over those of the permanent dipole moment. A time-dependent analysis of the reaction shows that the fluctuating barrier can occasionally be very low when the transition state is approached, allowing trajectories to be reactive with very low collision energies. [S1050-2947(96)08812-9]

PACS number(s): 33.80.Be, 42.50.Hz

I. INTRODUCTION

There is increasing interest in the possibility of using lasers to alter and/or control molecular reaction dynamics [1]. The effects of laser radiation on molecules have been studied in various spectral regions of laser radiation, from UV to IR (see, e.g., [2,3]). For optical and UV wavelengths, molecular dynamics can be altered by resonant excitation of *electronic* transitions. Such resonant mixing of different potential surfaces can facilitate molecular dissociation [4] or create new bound states [5]. For exchange reactions of the type $A+BC\rightarrow[ABC]\rightarrow AB+C$, resonant excitation to an upper potential surface (with low or no barrier) can allow reactants to overcome the barrier to reaction [6–8] on the ground-state electronic potential energy surface. Similarly, a laser catalysis scheme [9] suggested excitation to the upper potential surface before the transition state and deexcitation afterwards as another means of bypassing the reaction barrier.

For exchange reactions, the use of IR fields was studied by Orel and Miller [10] (see also Ref. [11]), who showed that an exchange reaction can be enhanced due to the interaction of a laser field with the permanent dipole moment of an $A+BC$ system, which is changing as the system crosses the transition state region. This can occur even if the reactants are infrared inactive. However, this absorption mechanism is inefficient if the laser cycle is either too long or too short compared to the characteristic time of reaction. For example, for the benchmark $H+H_2$ reaction and kinetic energies of $\sim 0.2-0.3$ eV, it becomes inefficient for the second harmonic of the CO_2 laser and higher frequencies [10].

In *intense* IR fields nonresonant mixing of the ground and excited electronic potential surfaces creates induced dipole moments in the reacting system. It has been recently recognized that such nonresonant mixing determines most of the features of intense-field dynamics of diatomic molecules in IR fields [12–16]. We show that, when applied to exchange reactions, interaction with an induced dipole moment increases reactivity. Reaction enhancement due to the induced dipole moment is free from the restrictions imposed on the laser frequency when a permanent dipole moment mechanism is used. Even for relatively high laser frequencies (i.e., when the laser cycle is much shorter than the time required for the system to cross the transition state) the enhancement of the reaction remains significant.

We also show that intense IR fields can induce bound states along the reaction path. Laser-induced bound states are important when dealing with cold molecules trapped and aligned by intense IR laser fields [17]. Such molecules open up new possibilities for the study of simple chemical reactions, since increasing the laser intensity can convert a simple bimolecular reaction into one which proceeds via an intermediate complex. Laser-induced bound states will appear not only in $A+BC$ exchange reactions, but also in the interaction of highly polarizable molecules, e.g., I_2 or Cl_2. Consequently, in molecular traps using intense IR fields the latter will induce bound complexes (perhaps even linear chains) of cold molecules, aligned and trapped by the same field.

There are several reasons for choosing infrared radiation, e.g., that of a CO_2 or Nd:YAG laser, as a means of promoting a chemical reaction. First, infrared frequencies are typically highly nonresonant with transitions between ground and first excited electronic states in simple molecules and atom-diatom reactions. Therefore, for exchange reactions in the ground state, the effect on the ground-state potential surface will be quite general and, in some aspects, simple. Second, one of the most important complications arising from intense-field effects — nonlinear ionization — is well understood in the infrared region, both for atoms and simple molecules [13,18–22]. Dissociation of simple molecules in IR

*Also at National Research Council of Canada, M-23A, Ottawa, Ontario, Canada K1A OR6 and Laboratoire de Chimie Théoretique, Faculté des Sciences, Université de Sherbrooke, Québec, Canada J1K2R1.

fields, which we want to avoid, has also been well studied [14,23,24]. Third, there is a great degree of flexibility in IR laser sources, in both intensity and pulse duration. Intensities can easily reach $I=10^{14}$ W/cm^2, a typical value at which rapid multiphoton ionization occurs (see, e.g., Ref. [18]). The pulse duration can vary by many orders of magnitude, from nanoseconds to femtoseconds. In the latter case the pulse duration is comparable to (or even shorter than) the time it takes for reacting molecules to pass through the transition state.

IR laser fields can align polarizable diatomic molecules quite well, even those without permanent dipole moments [17]. For example, at intensities $I\sim10^{13}$ W/cm^2 molecules such as Cl_2 or I_2 are aligned within an angle of $\pm20°$ (for rotational temperatures $\leqslant10$ K). Therefore, in strong fields a near-collinear geometry is much closer to reality than in the field-free case. In this paper we assume the limiting model of a collinear collision.

Some of the results presented in this paper have appeared in abbreviated form in two Letters. The first [25] introduced the formalism, reported a polarizability surface for collinear H_3, and described the lowering of the barrier due to the effect of the polarizability. It also reported the existence of bound states along the reaction coordinate. The second Letter [26] reported an *ab initio* dipole moment surface for collinear H_3 and examined the effect on the reaction probability of the interaction between the dipole moment and the laser field. The present paper gives a full account of these calculations, including the theoretical formulation, and examines the combined effects of both dipole moment and polarizability terms in the Hamiltonian.

The paper is organized as follows. The general approach is presented in Sec. II. In Sec. III we describe *ab initio* calculations of the dipole moment and polarizability of the collinear H_3 system and use these results to study the collinear $H+H_2$ exchange reaction in an intense infrared field. We first consider the case of a laser period much shorter than the characteristic time necessary to cross the transition state and then the case of a strong CO_2 laser, where the laser cycle is comparable to the time of motion through the transition state. Section IV summarizes our conclusions.

II. THEORETICAL MODEL

One of the most efficient methods of treating intense-field molecular dynamics is to apply the Born-Oppenheimer approximation to a *field-dressed* (see, e.g., [18]) system. This approach is often used in the case of optical frequencies, where Floquet potential surfaces are constructed [2,6]. However, for IR fields with intensities $I\geqslant10^{13}$ W/cm^2 the Floquet spectrum becomes highly complicated. Many field-free potential surfaces are involved in the interaction, each producing a dense manifold of new Floquet surfaces, all of which have to be included in the calculations. Both the physical clarity and the computational efficiency, characteristic to the Floquet approach at moderate and low intensities and visible or UV light, disappear at high intensities and IR frequencies, making the Floquet method impractical.

For laser frequencies that are much smaller than the characteristic frequency of the electronic transitions between ground and excited electronic surfaces, one can combine the Born-Oppenheimer approximation to the *field-dressed system* with the *quasistatic approximation* to the electronic dynamics [12–16,27]. This approximation is very successful in describing intense field processes in atoms and diatomic molecules in infrared fields [13–16,18,20,27,28]. For any instantaneous value of the IR electric field, $\mathcal{E}_0\cos(\omega_L t)$, we use the Born-Oppenheimer approximation and find the ground electronic potential surface in the constant electric field, considering the phase of the oscillating electric field as a parameter. The Hamiltonian of the system then becomes

$$H(t)=H_0-\mu\mathcal{E}_0\cos(\omega_L t)-\frac{1}{4}\alpha\mathcal{E}_0^2[1+\cos(2\omega_L t)], \quad (1)$$

where H_0 is the field-free Hamiltonian including nuclear motion, μ is the permanent dipole moment of the $A+BC$ system, α is its static dipole polarizability along the direction of the linearly polarized laser electric field, and ω_L and $\mathcal{E}_0$ are the laser frequency and the electric field strength, respectively. Both μ and α depend on the coordinates of the reacting system. In the model of a collinear collision which we use here, $\mu=\mu(r_{AB},r_{BC})$ and $\alpha=\alpha(r_{AB},r_{BC})$, where r_{AB},r_{BC} are the A-B and B-C internuclear distances, respectively. Unlike previous studies [10,11], we explicitly include the Stark shift, which is calculated in the quasistatic approximation. Electronic hyperpolarizabilities are not included in (1), but as long as quasistatic approximation is used and laser oscillations are included in Eq. (1), these higher order corrections do not become important until the laser intensity is very high: for the hydrogen atom this occurs at $I\approx1.0\times10^{15}$ W/cm^2 [29], well beyond the intensities discussed in this paper (see Sec. II C). The inclusion of these terms in (1) does not change our conclusions in any qualitative manner since they are corrections to the magnitude of the induced dipole, not alterations to its basic behavior.

As seen in (1), the three major effects of an intense field are (a) time-dependent interaction with the permanent dipole moment of the system; (b) time-independent modification of the ground-state surface due to the Stark shift; (c) time-dependent interaction with the field-induced dipole moment through the term proportional to $\cos(2\omega_L t)$. All three lead to interesting effects which we now discuss.

A. Time-independent shift

The time-independent part of the Stark shift $\alpha\mathcal{E}_0^2/4$ produces an overall change to the potential surface for the exchange reaction. As the molecule approaches the transition state, the electric field induces a larger dipole moment, since valence electrons can be moved across the whole atom-diatom complex. Therefore, in general we should expect the polarizability to increase as the system approaches the transition state.

The asymptotic behavior of the static polarizability at large distances between an atom and a diatomic molecule can be easily understood. An electric field induces a dipole moment in both the atom and the diatom. The induced dipoles are parallel to the direction of the field and, therefore, parallel to each other. They are given by the individual polarizabilities of atom and diatom: $d_a=\alpha_a\mathcal{E}_0$ and $d_{da}=\alpha_{da}\mathcal{E}_0$. The potential energy of the attraction of the two parallel collinear dipoles separated by the distance R is

$U(R)-U(\infty)=-2d_a d_{da}/R^3=-2\alpha_a\alpha_{da}\mathcal{E}_0^2/R^3$. The result is proportional to $\mathcal{E}_0^2$, just as are the individual Stark shifts in atom and diatom. Given the definition of polarizability, at large distances between the atom and the diatomic molecule we see that the total polarizability of the system is

$$\alpha(R)\sim\alpha_{da}+\alpha_a+4\alpha_a\alpha_{da}/R^3, \tag{2}$$

where $R\gg 1$ Å is the distance between the atom and diatom. The polarizability therefore increases as the transition state is approached. Consequently, the Stark shift increases and *the potential barrier for the reaction decreases*.

For symmetric systems, the formation of a covalent bond implies that the polarizability should reach a maximum along the reaction path at the transition state. Hence, the decrease of the potential barrier should be general for such systems. The importance of this effect, which decreases the threshold kinetic energy required for the reaction, is that it is almost frequency-independent. The only requirement is that the laser frequency should be small compared to the frequency of electronic excitation along the reaction path.

B. Time-dependent terms and the high-frequency limit

The system can absorb energy from the field due to the presence of $\cos(\omega_L t)$ and $\cos(2\omega_L t)$ in the Hamiltonian (1). In the first case the laser field interacts with the permanent dipole of the system. In the second case the laser field interacts with the induced dipole moment. Physically, the $\cos(2\omega_L t)$ term describes two-photon absorption via intermediate virtual excited electronic states, while unity in the square brackets in (1) corresponds to absorption followed by stimulated emission. Conditions for the energy absorption due to the $\mu\mathcal{E}_0\cos(\omega_L t)$ and $\alpha\mathcal{E}_0^2\cos(2\omega_L t)$ terms are, of course, different, not only because of the different oscillation frequencies, but also because of the different dependences of α and μ on r_{AB} and r_{BC}.

Qualitatively, the $[1+\cos(2\omega_L t)]$ term causes oscillations of the potential barrier between its field-free value V_0 and the maximum shifted value of $V_0-(1/2)\alpha\mathcal{E}_0^2$. The potential for vibrations perpendicular to the reaction path is also oscillating. If the laser period is much shorter than both the period of vibrations perpendicular to the reaction path and the characteristic time of the translational motion, the reactants see an average potential barrier, which is largely determined by $H(t)$ averaged over the laser cycle. That is, the time-independent shift $\alpha\mathcal{E}_0^2/4$ dominates over other modifications to the reaction surface. Below we refer to this as the ''high-frequency limit.'' In the opposite limit of laser period longer than or comparable to the time of crossing the transition state, a successful reaction may occur when the barrier is most suppressed $[1+\cos(2\omega_L t)=2]$, further lowering the reaction threshold. For the $H+H_2$ exchange reaction, Nd:YAG laser radiation ($10\,000$ cm^{-1}) corresponds to the high-frequency limit, while the CO_2 laser cycle (approximately 1000 cm^{-1}) is approaching the time scale of crossing the transition state region.

High-frequency limit

Mathematically, in the high-frequency limit the rigorous procedure for treating fast oscillating terms in the Hamiltonian (1) is based upon the Kapitza-Dirac method of separating fast and slow motions [30]. The Kapitza-Dirac method can be formulated using both classical and quantum theory, leading to identical results. It is routinely used in the theory of intense laser-atom interactions, where the main effect is the so-called ponderomotive potential (see, e.g., [18]), which is related to the spatial inhomogeneity of the laser intensity in the focus. In our case, the *ponderomotive-type* potential appears due to the dependence of both the permanent and the induced dipole moments on the nuclear coordinates.

Separation of the fast and slow motions is performed by introducing fast and slow variables:

$$r_{AB}=R_{AB}+\xi_{AB}\equiv R_{AB}+\xi_1,$$
$$r_{BC}=R_{BC}+\xi_{BC}\equiv R_{BC}+\xi_2. \tag{3}$$

Here $\xi_{AB}(t)$ and $\xi_{BC}(t)$ describe fast oscillations due to the rapidly oscillating terms in the Hamiltonian (1), *without* the time-independent part of the potential. The variables $R_{AB}(t)$ and $R_{BC}(t)$ describe the slow motion of the system. To derive the equations of motion for the slow variables classically, one has to substitute (3) into the classical equations of motion, use a Taylor expansion of the time-dependent and time-independent potentials around $R_{AB,BC}(t)$, and average the resulting equations over fast oscillations. Then one obtains the following effective *time-independent* Hamiltonian for $R_{AB,BC}(t)$:

$$H_{\rm eff}(R_{AB},R_{BC})=H_0(R_{AB},R_{BC})-\tfrac{1}{4}\alpha\mathcal{E}_0^2+U_p^{(1)}(R_{AB},R_{BC})+U_p^{(2)}(R_{AB},R_{BC}), \tag{4}$$

where the expressions for the ponderomotive-type potentials U_p depend on the choice of coordinates [30]. For R_{AB}, R_{BC} (distances between the nuclei along slow trajectories), $U_p^{(1)}$ has the form

$$U_p^{(1)}(R_{AB},R_{BC})=\frac{\mathcal{E}_0^2}{4\omega_L^2}\left[\frac{1}{M_{AB}}\left(\frac{\partial\mu}{\partial R_{AB}}\right)^2+\frac{1}{M_{BC}}\left(\frac{\partial\mu}{\partial R_{BC}}\right)^2-\frac{2}{M_B}\frac{\partial\mu}{\partial R_{AB}}\frac{\partial\mu}{\partial R_{BC}}\right], \tag{5}$$

where M_{AB} and M_{BC} are reduced masses and $\mu\equiv\mu(R_{AB},R_{BC})$ is the permanent dipole moment of the system. The potential $U_p^{(2)}$ is given by an equation similar to (5) with the following substitutions: $\mu\mathcal{E}_0$ should be replaced by $\alpha\mathcal{E}_0^2/4$, and ω_L should be replaced by $2\omega_L$. Hence, $U_p^{(2)}$ is proportional to $\mathcal{E}_0^4$ and is small compared to the field-free potential V_0 plus the time-independent part of the quadratic Stark shift and $U_p^{(1)}$, i.e., $U_p^{(2)}\ll V_0-\alpha\mathcal{E}_0^2/4+U_p^{(1)}$. We shall therefore omit $U_p^{(2)}$ below.

The coefficients in front of partial derivatives in (5) are the same as in the expression for the kinetic energy in coordinates r_{AB}, r_{BC}:

$$T=\frac{1}{2}\left[\frac{P_{AB}^2}{M_{AB}}+\frac{P_{BC}^2}{M_{BC}}-2\frac{P_{AB}P_{BC}}{M_B}\right]. \tag{6}$$

This property remains the same even if the mass-type coefficients in the kinetic energy T are coordinate dependent [30], e.g., if one uses ''natural collision coordinates'' [31].

As noted above, the results of (4)–(6) are the same when derived through quantum mechanics. The wave function Ψ is written as a product of the wave function $\mathcal{R}$, which depends on the slow variables R_{AB}, R_{BC} and describes the slow motion in the Hamiltonian, and the wave function Ξ, which depends on fast variables only and describes fast oscillations due to $\mu\mathcal{E}_0\cos(\omega_L t)$ and $\alpha\mathcal{E}_0^2\cos(2\omega_L t)$, without taking the rest of the potential into account.

Equations (4) and (5) are applicable if the amplitude of the fast oscillations $a_{\rm osc}$ is small compared to a characteristic size of the interaction region (about 1 Å). This leads to the following condition: $a_{\rm osc}\sim\mathcal{E}_0|\nabla\mu(S,x)|/M\omega_L^2\ll 1$ Å, where M is the effective mass along the reaction path. Although the value of M depends on the values of the natural coordinates, for an estimate one can use $M=\sqrt{M_A M_B M_C/(M_A+M_B+M_C)}$ [9]. If $a_{\rm osc}\sim 1$ Å, simple separation into fast and slow motions becomes impossible. Owing to the heavy mass in the denominator, for practical values of intensities and frequencies the oscillation amplitude remains small. For the $H + H_2$ reaction and CO_2 laser frequency, $a_{\rm osc}$ remains small until $I\sim 10^{15}$ W/cm^2, an intensity which the system cannot withstand owing to very efficient multiphoton ionization, which occurs in approximately 0.1 fs.

One of the most interesting features of the high-frequency limit is that the effective time-independent potential

$$V_{\rm eff}=V(R_{AB},R_{BC})-\frac{1}{4}\alpha(R_{AB},R_{BC})\mathcal{E}_0^2+U_p^{(1)}(R_{AB},R_{BC}) \tag{7}$$

can have local minima along the reaction path. These minima can appear due to increasing polarizability α as the reactants approach the transition state. Indeed, at large R the polarizability α increases as R^{-3}, i.e., much faster than the potential barrier. As we show below, these minima exist even for the $H+H_2$ reaction, where the reactants have relatively low polarizability and the reaction barrier is high. Second, for reactions with large variations of $\mu(R_{AB},R_{BC})$ these variations can yield minima in $U_p^{(1)}$.

C. Limits to laser intensity

In practice, the field intensity is limited by molecular ionization and/or dissociation. This is a problem in any laser-assisted chemical reaction which is typically resolved by the use of laser pulses. For simple molecules and strong IR fields both theory [23,24] and experiment [13,21,22] show that multiphoton ionization dominates multiphoton dissociation. Ionization in intense IR fields is well understood and can be described as tunneling in a time-varying electric field

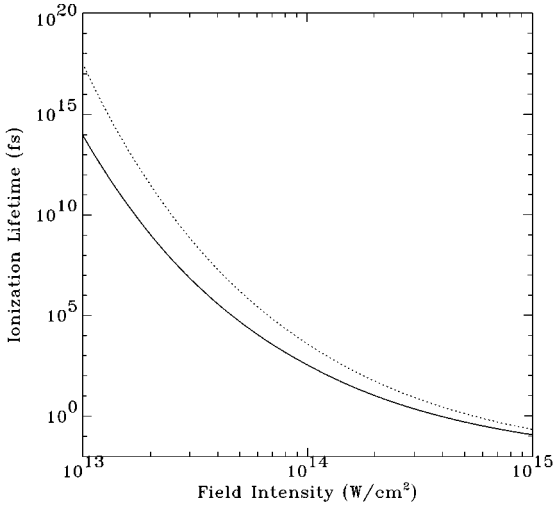

FIG. 1. Tunneling ionization lifetime of hydrogen atom (solid line) and hydrogen molecule (dotted line) in femtoseconds, as a function of laser field intensity. Note logarithmic scaling of both axes.

[13,18,19]. Simple analytical formulas for ionization rates give very good agreement with experimental data for both atoms [18] and diatomic molecules [13,18,19].

The rate of tunneling ionization is determined largely by the ionization potential of a system. Electron tunneling to the continuum is an instantaneous transition. Therefore, the effective ionization potential of a molecule is determined by the energy of a *vertical* transition from the ground state of the neutral system to the ground state of the ion. The rate of tunneling ionization in dc electric fields is given by the following well-known formula [13,18,19]:

$$w_i=A_{n^*,l,m}4I_p\left[\frac{2(2I_p)^{3/2}}{\mathcal{E}}\right]^{2n^*-|m|-1}\exp\left(-\frac{2(2I_p)^{3/2}}{3\mathcal{E}}\right), \tag{8}$$

where I_p is the ionization potential of the sytem, n^*,l,m are the effective principal quantum number, angular, and magnetic quantum numbers of the ionizing electron, and the coefficient $A_{n^*,l,m}$ given in [13,18,19] is $O(1)$ for $n^*\sim 1$. Using the quasistatic approximation, in an ac field $\mathcal{E}$ is substituted by $\mathcal{E}_0|\cos(\omega_L t)|$, so that $w_i\to w_i(t)$ depends on the phase $\omega_L t$ of the ac electric field. Typically, $w_i(t)$ is then averaged over the laser cycle.

The characteristic upper limits for intensities are given by the following example of an $H+H_2$ reaction: at $I=7\times 10^{13}$ W/cm^2 the hydrogen atom ionizes in $\tau_i\approx 5$ ps (see Fig. 1), and at $I=5\times 10^{13}$ W/cm^2 ionization of a hydrogen atom takes $\tau_i\approx 80$ ps. The hydrogen molecule is much more stable with respect to ionization due to its higher effective ionization potential for a vertical transition (Fig. 1). To avoid ionization, short laser pulses should therefore be used, e.g., a 1-ps pulse for $I=7\times 10^{13}$ W/cm^2. This leaves enough time for the reaction, which takes about 100–200 fs near threshold. Those collision partners which do encounter each other during the pulse should therefore show evidence of different reactivity (see Sec. III below). Note that short femtosecond

IR pulses are readily available in the intense field regime, including square-shaped 100–200 fs pulses for a CO_2 laser [32].

III. APPLICATION TO COLLINEAR H+H_2

In this section we apply the general approach described above to the benchmark collinear H+H_2 exchange reaction. The section consists of three parts. In Sec. III A we describe *ab initio* calculations needed to obtain the dipole moment and the polarizability surfaces for the collinear H+H_2 reaction. In Sec. III B we study the ''high-frequency'' limit of the reaction dynamics on the modified potential surface. That is, we examine the reaction dynamics for the effective time-independent Hamiltonian given by Eqs. (4)–(7). In Sec. III C, we examine the reaction dynamics in the field of a CO_2 laser, where the laser period is approximately on the same time scale as that of the nuclear motion across the transition state. Here the time-dependent terms in (1) become important.

A. Structure calculations

A field-free potential energy surface for collinear H_3 based on the *ab initio* calculations of Liu and Siegbahn and the fitting function of Truhlar and Horowitz (LSTH surface) [33] was used in these calculations. This surface has accurate asymptotic properties for H_2, including a zero-point energy of 0.271 eV (expt. 0.270 [34]). The classical barrier occurs at $R_{AB}=R_{BC}=1.757$ bohr, where $E=0.428$ eV relative to reactants H + H_2.

1. Permanent dipole

The permanent dipole moment was calculated using the GAUSSIAN-92 program package [35], with a quadratically convergent configuration interaction method and a basis set (Basis I) which includes diffuse and multiple polarization functions [the method and/or basis is denoted QCISD/6-311++G($3df$,$3p$), corresponding to a $4s3p$ basis for hydrogen]. Points were calculated with a grid spacing of 0.25 bohr over the range $1.0 \leqslant R_{AB},\ R_{BC} \leqslant 5.0$ bohr where the dipole moment varied strongly, and over a sparser grid with spacing 0.5 bohr in the region $5.0 \leqslant 10.0$ bohr, where the dipole moment varies slowly and becomes asymptotically zero. Values at the grid points were fitted to a two-dimensional natural cubic spline to provide interpolated values at any coordinate pair.

Figure 2(a) shows the component of the permanent dipole moment μ_z (in a.u.) along the internuclear (and laser field) axis, mapped vs the coordinates R_{AB} and R_{BC} over the range $1.0 \leqslant (R_{AB},R_{BC}) \leqslant 5.0$ bohr, the region where the interaction becomes significant. The absolute sign of the dipole moment is arbitrary, depending on the choice of the positive direction of the coordinate system. The surface shows a rather complex behavior, characterized by the following features: the maximum (absolute) value of μ for H_3 occurs in the energetically inaccessible region near $(R_{AB},R_{BC}=1.5,1.0)$ where $|\mu| \approx 0.24$ a.u. A smaller local extremum occurs near (3.5,2.8), where $|\mu| \approx 0.03$ a.u. Zeros of the dipole moment occur along the symmetric stretch coordinate $R_{AB}=R_{BC}$ where the dipole is zero by symmetry, while the other is normal to it [the zero contour line is labeled in Fig. 2(a)]. Thus zero contours of the dipole moment must be crossed by the system several times in going from reactants to products.

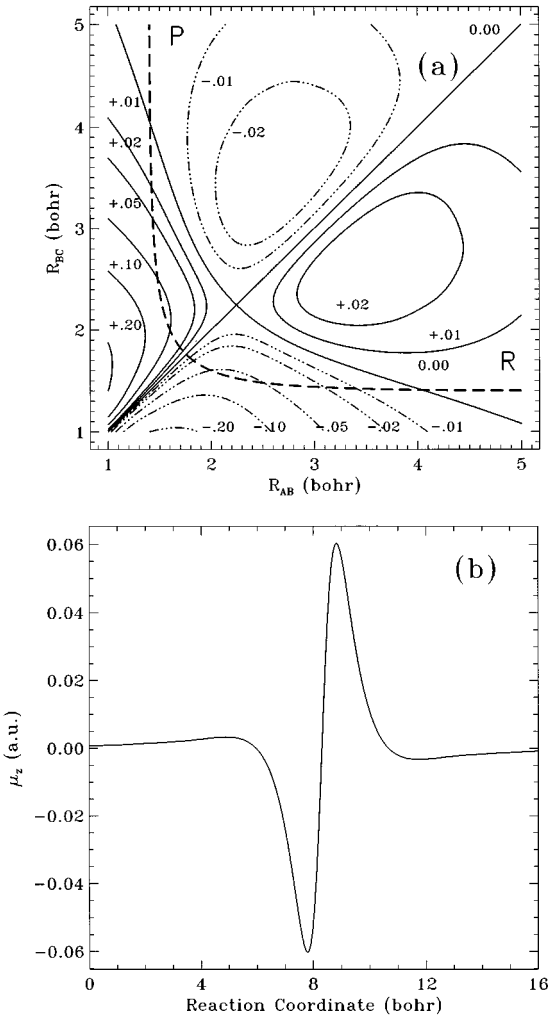

FIG. 2. Permanent dipole moment μ_z along the internuclear axis of collinear H_3, in a.u.: (a) full surface showing contour values of μ_z as a function of (R_{AB},R_{BC}); (b) variation of μ_z along the minimum energy reaction path [dashed line from reactants R to products P in (a)].

The variation of the dipole moment along the minimum energy reaction path is shown in Fig. 2(b), corresponding to the reaction coordinate connecting the reactant (labeled R) and product (labeled P) regions of Fig. 2(a). Along this path, the dipole moment starts out (weakly) positive, changes sign, and reaches a minimum of -0.06 a.u., eventually returning to zero at the symmetric transition state. The opposite behavior is observed when the dividing line $R_{AB}=R_{BC}$ is crossed. The fact that along the reaction coordinate the calculated dipole moment changes sign prior to reaching the transition state should have little effect on the reaction dynamics due to the small magnitude of $|\mu|$ at large R. It was not present, however, in the simpler model function assumed by Orel and Miller [10].

The variation of the dipole moment along the reaction coordinate may be understood by analogy to the diatomic molecule HeH, which corresponds to the limit of either

TABLE I. Comparision of polarizability calculations with available literature values. Column 2 refers to the present work (shown in Fig. 3) while column 3 refers to higher quality test points.

	Polarizability values α_{zz} along the internuclear axis (in a.u.)			
Species	QCIS/Basis I	QCIS/Basis II	Exact	Ref.
H atom	3.7703	4.4649	4.5000	[38]
H_2 ($R=1.40$ bohr)	6.4507	6.4142	6.3873	[40]
H_3 ($R=1.757$ bohr)	21.9838	21.8072	.	

R_{AB} or R_{BC} approaching zero. The HeH system shows a maximum in the value of μ at short separations followed by a change in sign, a minimum, and an asymptotic approach to zero at large separations [36]. This is the same qualitative behavior as is observed in Fig. 2(b).

The accuracy of the *ab initio* calculations was checked at the two extrema described above by comparison to more extended treatments, which involved either expanding the basis set or using a more complete CI treatment or both. A larger $6s4p1d$ basis set described by Peng *et al.* (Basis II) [37] was used for these comparisons. First, the full CI (configuration interaction with all single, double, and triple excitations) dipole moment was calculated with Basis I at both geometries to determine the effect of excluding triple excitations from the QCISD wave function. The QCISD/Basis I values differed from the full CI/Basis I values by less than 4%, indicating that omission of triple excitations does not cause substantial error. Next, the effect of augmenting the basis set was tested by comparing the QCISD dipole moments from Basis I to the complete singles and doubles CI (denoted CISD) result of Basis II. The μ(QCISD) values of Basis I differed by less than 5.0% from the CISD values of Basis II. The QCISD/Basis I dipole moment surface presented in Fig. 2 is therefore expected to be close to the exact limit in the region accessible to low energy collisions.

2. Polarizability

The static polarizability component α_{zz} along the molecular axis for collinear H_3 was generated using the method, basis set, and grid spacing identical to that used to generate the dipole moment, i.e., QCISD with Basis I. The accuracy of the calculated polarizability is sensitive to the choice of basis set, particularly with respect to the inclusion of diffuse functions [38,39]. Table I shows the calculated values for H, H_2, and H_3. The static polarizability of the hydrogen atom is known analytically to be 4.50 a.u. [38]. In contrast, the atomic polarizability with Basis I was found to be only 3.77 a.u. This low result was found to be caused by the lack of a sufficiently diffuse p function, the smallest of which is $\zeta=0.1875$ in Basis I. When Basis II is used, which includes such Rydberg p functions, the result differed from the exact limit by only 0.04 a.u.

Based on the atomic calculations, one would expect Basis I to produce a poor surface for the molecular system. This is not the case, however, as we found that the molecular calculations are much more accurate than those for the isolated atoms. The improvement is due to the presence of diffuse s functions in Basis I ($\zeta=0.036$ [35]), which are able to combine on different centers to allow polarization along the bond, i.e., effectively creating a diffuse polarized basis set. For H_2, comparison can be made between our calculations and the near-exact results of Rychlewski [40]. In Table I, the polarizability values quoted are measured along the molecular axis. For H_2 the QCISD method using Basis I differed from the reference result of 6.39 a.u. by only 0.06 a.u., and the Basis II result gave a result to within 0.03 a.u. The Basis I results remain close to the near-exact values over the range 1.0–4.0 bohr, the maximum difference never exceeding 2%. Therefore, a polarization basis is provided by antisymmetric combinations of the $2s$ functions in the basis, effectively simulating the necessary $2p$ character, when the atomic orbitals are able to overlap, as in this region.

The same basis set combination effects also apply to the H_3 system, explaining the rather good agreement between the basis sets used. Results were obtained for H_3 at the transition state geometry (collinear, with equidistant bonds of $R = 1.757$ bohr). The difference between the QCISD values of Basis I and Basis II was only 0.18 a.u. In addition, these results did not vary appreciably with inclusion of triple excitations by the QCISD(T) method, i.e., the latter method increased the H_3 polarizability calculated with QCISD/Basis I by 0.04 a.u.

Figure 3(a) shows the polarizability α_{zz} mapped vs (R_{AB},R_{BC}) for the range 1.0–5.0 bohr. The minimum energy path is also shown on this diagram [dashed line from reactants to products, as in Fig. 2(a)].

The polarizability increases along the minimum energy path from reactants to transition state. There is a saddle point in polarizability located near the transition state (equidistant, $R=1.5$ bohr). The polarizability increases to the global maximum along the diagonal, near $R_{AB}=R_{BC}=3.2$ bohr, where α_{zz} is $\sim$ 33 a.u. Note that the bond distance for which the maximum in polarizability occurs for H_3 is very close to that where the maximum occurs in H_2.

Figure 3(b) shows how the polarizability varies along the reaction path from $\sim$ 10.3 a.u. at the H + H_2 asymptote to $\sim$ 22 a.u. at the transition state. Due to the error in the atomic polarizability of H (3.77 vs 4.5 a.u.), the H + H_2 asymptote lies too low by this amount. The value of the H_3 transition state, in contrast, is much more accurate. The result is that the change in polarizability along the reaction coordinate from reactants to transition state in our calculation is too large; the calculated variance is 11.76 a.u. while the exact value is estimated to be 10.92 a.u. The latter is obtained by using the exact values of H and H_2 with the QCISD/Basis II value for the transition state. This difference will cause a minor effect on the reactivity, but qualitatively all of our conclusions are insensitive to this error.

Comparing the permanent dipole moment and the polarizability along the reaction path [Fig. 2(b) and Fig. 3(b)], one

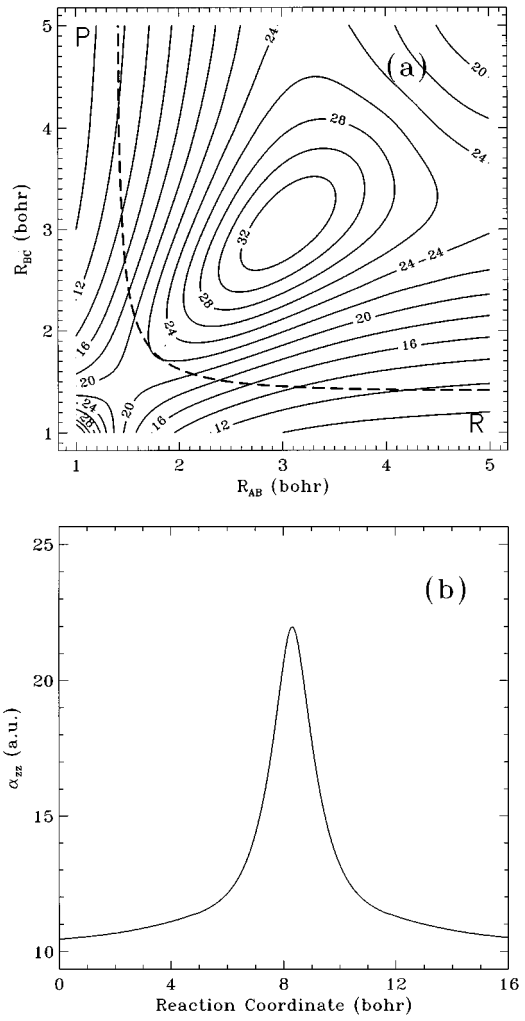

FIG. 3. Static polarizability component α_{zz} along the internuclear axis of collinear H_3: (a) full surface out to 5.0 bohr, showing contour values in a.u.; (b) variation of α_{zz} along the reaction path in a.u. [dashed line from R to P in (a)].

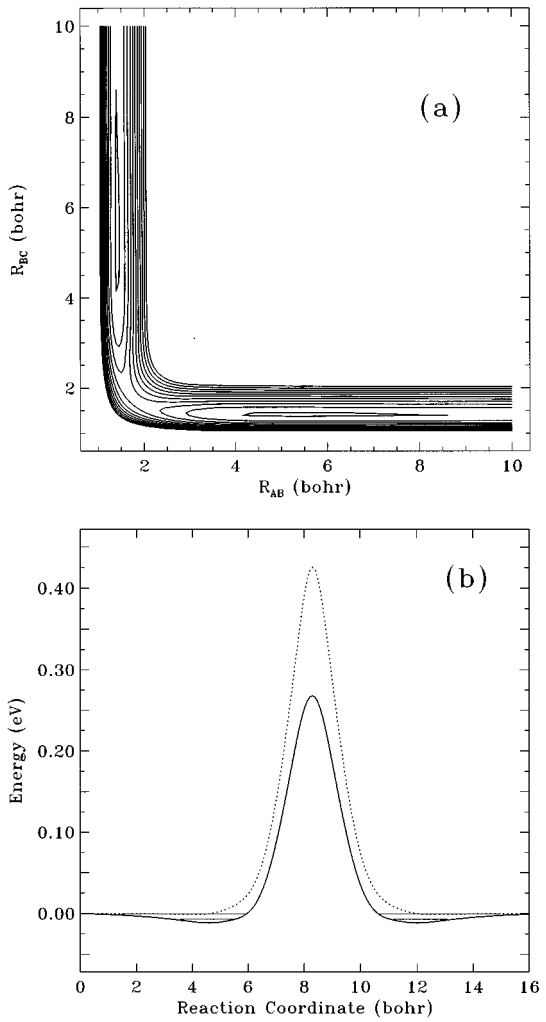

FIG. 4. Potential energy surface for the collinear $H+H_2$ reaction in the high-frequency limit [Eq. (4)], at $I=7\times10^{13}$ W/cm^2: (a) Contour plot with lines from 0.0 eV to 1.0 eV in 0.1 eV steps. Energy zero corresponds to the $H+H_2$ asymptote; (b) potential energy along the minimum energy reaction path. Dashed line, no field; solid line, with the field. Field-induced bound states are shown for $D+D_2$ mass combination.

can see that the variation of the Stark shift along the reaction path, which is $(1/2)\Delta\alpha\mathcal{E}_0^2$, approaches $\hbar\omega_R=\mu_{\max}\mathcal{E}_0$ at the intensity of only $I\approx3.5\times10^{12}$ W/cm^2 ($\mu_{\max}$ is the maximum value of the permanent dipole moment along the reaction path [10]). In the region of intensities where $\hbar\omega_R$ becomes significant, i.e., $I>10^{13}$ W/cm^2, the Stark shift dominates the laser interaction terms in the Hamiltonian. This becomes even more true in the high-frequency limit, when the term due to the permanent dipole moment effectively averages out of the Hamiltonian (1).

B. Reaction dynamics in the high-frequency limit

As explained in Sec. II, in the high-frequency limit the effective Hamiltonian becomes time-independent [Eq. (4)]. For the $H+H_2$ exchange reaction the high-frequency limit is realized, e.g., for the Nd:YAG laser frequency, and the frequency required to achieve the high-frequency limit decreases with increasing mass of the reactants. The contribution of the ponderomotive-type potential $U_p^{(1)}$ [Eq. (5)] is negligible for this system.

Figure 4(a) shows the effective potential surface for the reaction [Eq. (7)] at a laser intensity $I=7\times10^{13}$ W/cm^2. The surface still resembles the field-free LSTH surface [33] except that a new feature is present: there is a potential energy well located in the reactant (product) valley at R_{AB} (R_{BC})$=5.35$ bohr. The center of the well lies at R_{BC} (R_{AB})$=1.41$ bohr, i.e., the undistorted H_2 internuclear distance, so that this bound species is very much like reactants $H + H_2$.

Figure 4(b) shows the field-free (LSTH surface) and field-dressed (LSTH surface modified by the Stark shift) potential curves along the reaction path. As expected, *the laser-induced Stark shift lowers the potential barrier for the reaction*. At $I=7\times10^{13}$ W/cm^2 it is lowered by $\sim$ 33% of its height, or 0.14 eV.

Figure 4(b) also shows that *the laser field induces potential minima before and after the potential barrier*. This is caused by the change in polarizability along the reaction

path. For $D + D_2$ these minima become deep enough to support a bound state at $I \approx 5 \times 10^{13}$ W/cm^2. At this intensity ionization occurs in about 80 ps (Fig. 1), so the ionization lifetime of the field-induced bound state is relatively long. Since the potential minimum occurs at (5.35, 1.41) [see Fig. 4(a)] bohr, to a first approximation the bound states of the collinear $D + D_2$ ($H + H_2$) system can be written as a product of D_2 (H_2) vibrations and motion along the reaction coordinate. The depth of the potential well at $I = 7 \times 10^{13}$ W/cm^2 is 94 cm^{-1}, and the zero-point energy for $H+H_2$ system is 49 cm^{-1}, while for the $D+D_2$ system there are two bound levels with energies 37 cm^{-1} and 88 cm^{-1} above the potential minimum.

It is the relatively long-range R^{-3} asymptotic behavior of the polarizability that is responsible for creating new bound states along the reaction path. The potential barrier near the transition state falls exponentially at large R, and the R^{-3} behavior of the Stark shift dominates the potential surface. Physically, the field induces a van der Waals–type force, which has a longer range than the usual van der Waals force (R^{-6}).

From Fig. 4(b) it is clear that the reactivity on the field-free LSTH surface and the laser-modified surface will be different. Following [10,11], quasiclassical trajectory calculations were carried out at field strengths of zero (unmodified LSTH surface) and 7×10^{13} W/cm^2, to determine the collinear reaction probability as a function of collision energy. Details of the field-free trajectory calculation have been described in the literature [41–43]. The quasiclassical results must be averaged over the initial conditions. For the high-frequency case, when the effective Hamiltonian is time-independent, these include size of the reaction shell, BC (H_2) vibrational phase, and relative translational energy of A with respect to the center of mass of BC (denoted E_T). The reaction shell center-of-mass distance $R_{\text{c.m.}} = R_{AB} + R_{BC}/2$ is chosen to be in the noninteraction region, with $R_{AB} = 5.0$ Å. Initially, the BC oscillator has its zero-point vibrational energy in the potential modified by the Stark shift (0.265 eV vs 0.271 eV on the field-free LSTH surface). Sampling of the BC (H_2) oscillator was done at 200 points spaced uniformly in time over the period of one vibration. The energy resolution in relative translational energy E_T was chosen to be 0.01 eV, so that energy thresholds were determined to within this amount. The resulting trajectory outcomes were averaged over initial BC vibrational phase to obtain the collinear reaction probability $P_R(E_T)$.

Figure 5 shows that the reaction threshold E_0 has been lowered on the modified surfaces, as expected. The field-free collisional energy threshold E_0 (minimal E_T for reaction) is 0.28 eV, in good agreement with the calculations of Mayne [43], while the high-frequency result for $I = 7.0 \times 10^{13}$ W/cm^2 is 0.14 eV. It can also be seen that the reaction probability near threshold is lower than for the unmodified surface. The reason for this lowered reaction probability has to do with the shape of the modified surface near the transition state, but since the one-dimensional rate constant is dominated by the threshold behavior, *it is clear that the rate constant will be strongly enhanced for the surfaces with the lowered barriers*. Due to the very low polarizability of the system under consideration, the intensities used here are quite high. This limits the pulse duration to $\tau \sim 1$ ps to avoid

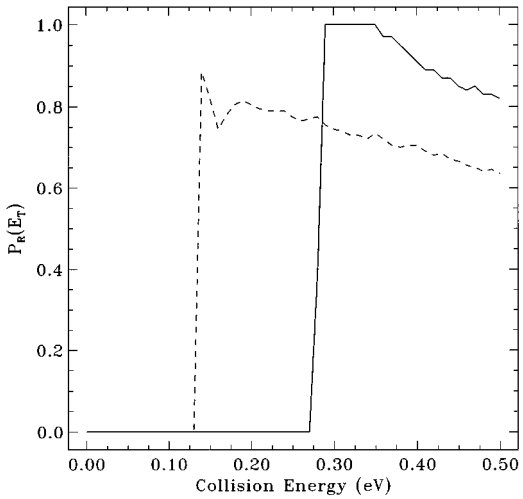

FIG. 5. Quasiclassical collinear reaction probability $P_R(E_T)$ as a function of collision energy E_T. Solid line: field-free LSTH surface. Dashed line: high-frequency limit at $I = 7 \times 10^{13}$ W/cm^2.

ionization. Consequently, the collision probability during the pulse is low. However, the surface effects discussed here yield an exponential dependence in the one-dimensional rate constant, while the collision probability enters as a preexponential factor. For a Boltzmann distribution, the gain in the exponential factor is $R = \exp(\Delta E_0 / kT)$. For the $H + H_2$ exchange reaction, with laser intensity $I = 7.0 \times 10^{13}$ W/cm^2, $R = 10^2$ at $T = 300$ K, while at liquid nitrogen temperature (77 K) $R = 10^9$. For molecules such as halogens, where the polarizability is an order of magnitude larger, the required intensity is lowered by a factor of 10. The ionization lifetime thus moves well into the nanosecond range.

Figures 6(a) and 6(b) show reactivity maps [41,44], which give the dependence of the reaction result on the initial phase of the BC oscillator, both with and without the laser field. In this polar plot the radial coordinate is the translational kinetic energy E_T and the polar phase is the initial phase of the BC oscillator ϕ_v (for mapping purposes the 200 points uniform in time map into vibrational phase, i.e., the first 50 points correspond to 0°–90°, etc.). Reactive trajectories are represented by black dots, while the white areas correspond to the nonreactive trajectories. The changes in the band structure reflect significant differences in the classical dynamics, which are caused by the changes in the potential surface. The most obvious effect shown on the reactivity maps is the lowered threshold E_0 [narrower inner area on Fig. 6(b) relative to Fig. 6(a)]. Other interesting effects are also present, however. In the absence of the laser field we have broad continuous bands with thin chattering regions at the boundaries between reactive and nonreactive regions. This picture changes radically in the presence of an intense laser field. As a result of the modifications to the potential energy surface, the continuous structure of the reactive bands at low energies is nearly destroyed, resulting in reactive and nonreactive bands which become very thin. The boundary regions correspond to activation of the symmetric stretch mode at the transition state. The trajectory can then end up on either side of the reaction barrier [44] with only slight changes to the initial conditions. Overall, the described change to the reactivity

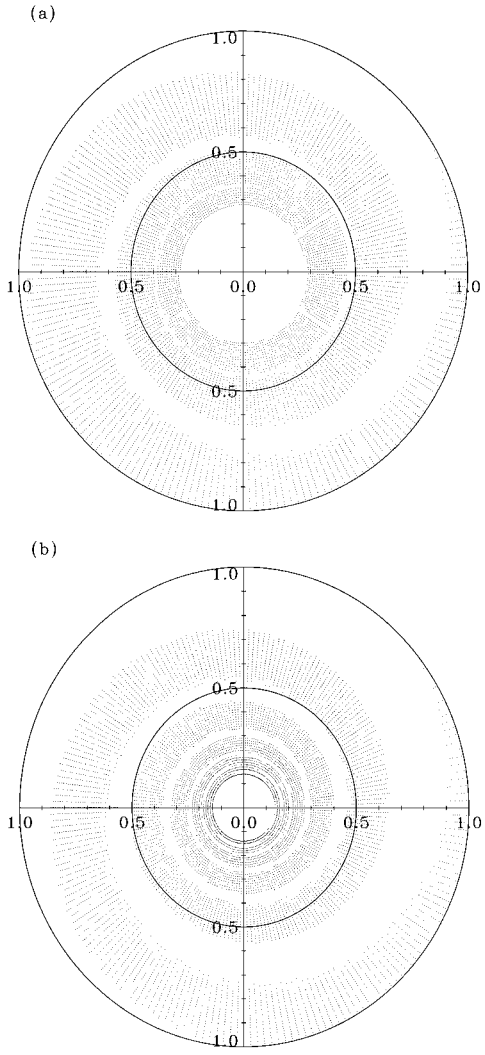

FIG. 6. Reactivity maps for collinear $H+H_2$ reaction, showing the reaction outcome as a function of collision energy (radial coordinate) and BC vibrational phase (angular coordinate): (a) field-free LSTH surface, right map; (b) high-frequency limit with $I=7\times10^{13}$ W/cm^2. Black regions indicate a reactive trajectory, white regions are nonreactive.

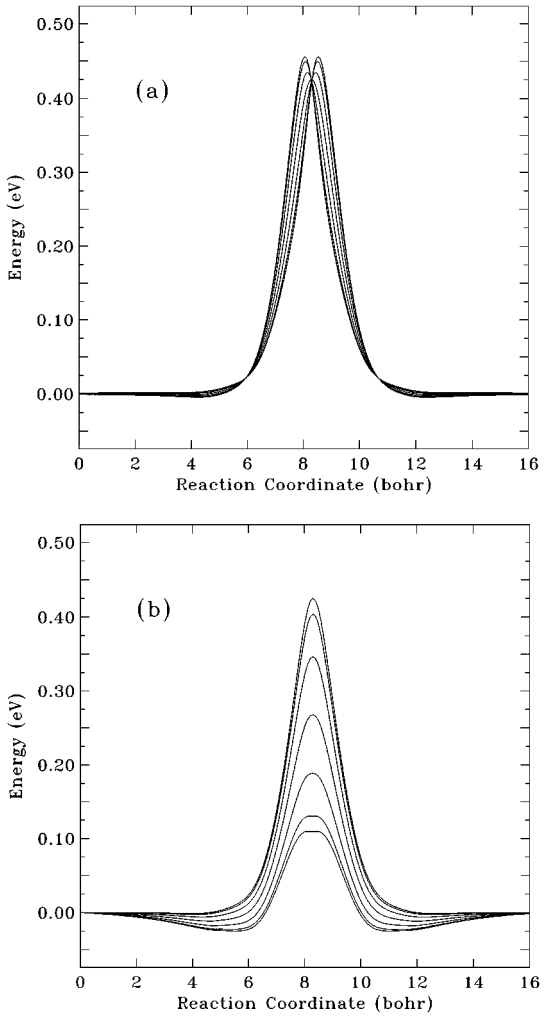

FIG. 7. Snapshots of the energy profile along the reaction coordinate as the laser goes through one period of its oscillation, for $I=7.0\times10^{13}$ W/cm^2: (a) LSTH surface plus inclusion of only the permanent dipole moment interaction, (b) LSTH surface plus inclusion of only the polarizability.

maps reflects increasingly chaotic reaction dynamics. Similar effects of high-intensity laser fields have been described in a time-dependent treatment in [11], however in our case the effect occurs on a *time-independent* surface. It arises from the flattening of the barrier in the region of the transition state, causing a loss of selectivity in trajectories which lead to products. This same loss of selectivity results in reaction probabiliites near threshold which are below 1.0 on the laser-modified surface, i.e., trajectories crossing a broad flat saddle point are easily reflected back to reactants, whereas those which traverse a narrow steep saddle (field-free surface) are strongly focused towards products.

C. $H+H_2$ reaction in an intense CO_2 laser field

To simplify the discussion, we will first describe the effects of the time-dependent terms $\mu\cdot\mathcal{E}_0\cos(\omega_L t)$ and $\alpha\cdot\mathcal{E}_0^2\cos(2\omega_L t)$ separately, and then present the combined results.

Formally, the time-dependent terms of Eq. (1) change the classical equations of motion through the addition of terms of the form $(\partial\mu/\partial R)f(t)$ and $(\partial\alpha/\partial R)g(t)$, where $f(t)$ and $g(t)$ are the time-dependent $\mathcal{E}$ and $\mathcal{E}^2$ terms, respectively. These additional terms correspond physically to the familiar processes of infrared and Raman absorption, respectively. Complete analysis of a laser-assisted process requires (i) monitoring the energy absorption and/or loss along the trajectory, which depends on the gradient of dipole moment and polarizability as well as the laser phase, and (ii) monitoring the change in potential energy of the system due to the added terms in the classical Hamiltonian. A conceptually simple but useful model considers only the latter, i.e., the potential energy of the system is examined at ''snapshots'' in time, and the effect on the dynamics is inferred from the change in potential energy with time.

Figure 7(a) illustrates this approach by showing the potential energy profile along the reaction coordinate of collinear H_3, where only the permanent dipole moment interaction term is included. Each curve represents the minimum energy reaction path for a fixed laser phase, i.e., a fixed value of

$\cos(\omega_L t)$. The laser phase is shown for several increments over an entire laser cycle. Since the dipole moment is an odd function of reaction coordinate with an inflection point at the transition state [Fig. 2(b)], the energy along the $R_{AB}=R_{BC}$ line (which formerly contained the field-free transition state) cannot change. In other words, the energy at the LSTH transition state ($R_{AB}=R_{BC}=1.757$ bohr) cannot be different from its original value. However, the position of the transition state along the reaction coordinate changes when the laser field is present. This is shown in Fig. 7(a), where a higher barrier is encountered either before or after the LSTH transition state geometry. The mechanism of threshold lowering in terms of this oscillating surface picture is now a question of correct timing: it is possible for the surface to rise up behind the mass point characteristic of the reacting system and impart momentum in such a way as to accelerate it across the saddle point. When viewed in this light, it is clear that this mechanism will be sensitive to the laser frequency and should be inefficient in the low- and high-frequency limits.

Figure 7(b) shows the reaction coordinate of the collinear H_3 surface over the course of a laser cycle, with only the correction due to the polarizability (no dipole moment term present). The barrier height is never higher than its field-free value (0.428 eV [33]). The high-frequency limit [see Fig. 4(b)] gives the middle curve, of height 0.27 eV. Trajectories will be reactive below the high-frequency limit energy threshold if they arrive at the transition state at a time when the barrier is in the low turning point of its oscillation.

For the 1000 cm^{-1} radiation of a CO_2 laser, the time scales of laser oscillation and translational motion across the transition state are comparable. As is clear from Fig. 7, the result of the collision is therefore sensitive to the laser phase when the system approaches the transition state. Hence, the problem has an additional degree of freedom, the initial phase of the laser field at time zero. Using a sampling grid over the laser phase of 7.5° (48 sample points), the averaged results of quasiclassical trajectory calculation were obtained. The actual value of the laser frequency used for these trajectory calculations was 945 cm^{-1}. The remaining initial conditions, including the grid of E_T values and the 200 sample points for the BC oscillation phase, were identical to those used in Sec. III B.

Results of the trajectory calculations for various combinations of interaction terms in the potential, and averaged over laser phase, are shown in Fig. 8. Figure 8(a) compares the field-free (LSTH) dynamics with those obtained using the LSTH + dipole moment (time-dependent) term, and the LSTH + polarizability (time-dependent) term. The variation of the reaction probability using the *ab initio* dipole moment surface [shown as a dotted line in Fig. 8(a)] is remarkably close in form to that obtained by Orel and Miller [10]. Thus their simplified treatment and model function of the dipole moment can be considered to be essentially correct, although the magnitude of the *ab initio* dipole moment presented here is considerably smaller than they assumed. The lowering of the energy threshold for reaction is 0.07 eV from the dipole contribution, and 0.18 eV from the polarizability contribution. Thus we see, as indicated earlier, that the polarizability correction has a much larger effect on the reaction dynamics.

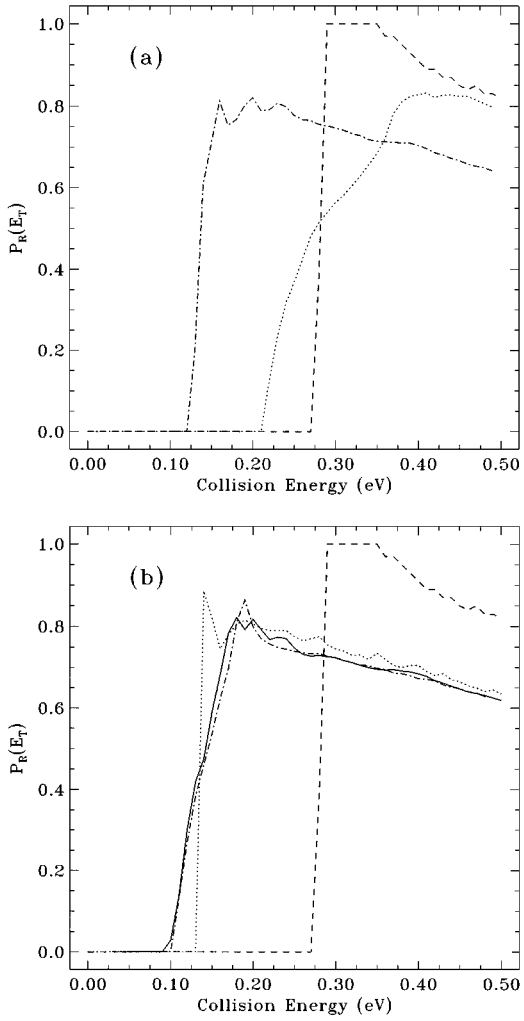

FIG. 8. Collinear H + H_2 reaction probability for $I=7\times10^{13}$ and $\omega_L=945$ cm^{-1} for various calculations: (a) Field-free (dashed line); plus dipole contribution only (dotted line); plus polarizability contribution only (dashed-dotted line). (b) Field-free (dashed line); high-frequency limit (dotted line); high-frequency limit + dipole contribution (dashed-dotted line); full calculation (solid line).

Figure 8(b) shows, in addition, reaction probabilities for the high-frequency limit (Stark shift contribution), the high-frequency limit plus dipole moment correction, and the full calculation. The latter includes all terms in the Hamiltonian, i.e., the full time-dependent contributions from both dipole moment and polarizability. The high-frequency limit (dotted line) shows a substantial lowering of the threshold (0.15 eV) and a shape which is similar to that obtained in Fig. 8(a) for the time-dependent polarizability only. A further small lowering results from the dipole contribution (0.03 eV). Finally, the full calculation shows the lowest energy threshold reported here, which is $E_0 = 0.10$ eV. Thus the energy threshold for reaction has been lowered substantially, from its original field-free value of 0.28 eV to its minimum value of 0.10 eV. Very little collision energy is therefore needed in the full calculation in order to show some reactive trajectories.

Comparing the various curves in Figs. 8(a) and 8(b), we see that very little change in the reaction probability is intro-

duced by the time-dependent part of the Stark shift; E_0 is lowered by only 0.02 eV from the threshold of the high-frequency limit. The reason for this is that the frequency $2\omega_L$ is too high even if the CO_2 laser is used. Since ω_L is not large enough to be considered in the high-frequency limit, the main features of the full calculation are reproduced by the partial calculation of the high-frequency limit Stark shift and the permanent dipole moment [dashed-dotted line in Fig. 8(b)]. The effect of the dipole moment is now less than when it was considered by itself. The threshold lowering of the dipole in the partial calculation is only 0.03 eV below the value of the high-frequency limit. This further serves to illustrate that, while the dipole contribution will become negligible in the high-frequency limit, the Stark shift caused by the induced dipole moment will remain in effect over a large range of laser frequencies.

IV. CONCLUSION

We have examined the effect of the laser-induced dipole moment on the structure of the potential energy surface and the probabilty of $H + H_2 \rightarrow H_2 + H$ exchange in an intense nonresonant IR laser field. We found that the laser field not only reduces the classical barrier to reaction but also induces bound states along the reaction path. The enhancement mechanism described here is based on the increase in the Stark shift as the reactants approach each other. At large distances such an increase reflects the mutual attraction of the two dipoles induced in the reactants by an intense low-frequency laser field.

In general, there will be two sources of enhancement of a reaction in infrared fields: (i) interaction with the permanent dipole moment, and (ii) interaction with the induced dipole moments. For the $H + H_2$ reaction, the values of the *ab initio* permanent dipole moment are very low. When the laser cycle matches the time of crossing the transition state [10], the reduction of the threshold E_0 due to $\mu \cdot \mathcal{E}$ is [10] $\Delta E_0 \sim \hbar\omega_R = |\mu_{\max}|\mathcal{E}$, where $\mu_{\max}$ is the maximum value of the dipole moment along the reaction path. From Fig. 2 at intensities $\sim 10^{13}$ W/cm^2 the value of $\hbar\omega_R$ is only 0.03 eV, and hence the reduction of the threshold due to the permanent dipole moment is small. At higher intensities the Stark shift dominates laser-introduced modifications of the reaction dynamics. Furthermore, the reaction enhancement due to the interaction with a permanent dipole moment is only significant when the laser cycle approximately matches the time of crossing the transition state. This is in contrast to the laser-induced dipole moment, which yields significant enhancement even in the high-frequency limit.

One of the most important properties of the described enhancement mechanism in the high-frequency limit is that it is quite general. It is based on the Stark shift, which occurs in all systems, and the increase of polarizability in the vicinity of the transition state, which is also expected to be a typical phenomenon for covalent processes. Although the $H+H_2$ system is only weakly polarizable, the effect is already present even for this reaction. If an intensity of $I = 5\times 10^{13}$ W/cm^2 is used, the reaction threshold E_0 is reduced by 0.1 eV, which is an observable amount. Highly polarizable systems, such as halogens, are expected to demonstrate much stronger effects. The gain in the one-dimensional rate constant $R = \exp(\Delta E_0/kT)$ is larger for cold molecules. For $H + H_2$, the gain is two orders of magnitude at room temperature and nine orders of magnitude at liquid nitrogen temperature. We stress that cold molecules in intense IR laser fields are of significant interest for trapping and alignment schemes [17].

The major factor limiting the intensity that can be applied is multiphoton ionization. For halogens with the polarizability approximately an order of magnitude higher than for hydrogen, the intensity required to significantly reduce the reaction threshold would be an order of magnitude lower than that studied here. As a result, the lifetime of the reacting systems with respect to ionization will move well into the nanosecond range.

Laser-induced minima along the reaction path are another interesting result of the interaction with IR field. For well-polarizable molecules such as I_2, the potential well for two interacting iodine molecules can become comparable to kT at room temperature for intensities below 10^{13} W/cm^2. A simple estimate shows that for collision of two I_2 molecules the energy of attraction is $\Delta U(R) = 0.03$ eV at $I = 3.5\times 10^{12}$ W/cm^2 and $R = 6$ bohr, a typical distance at which field-free molecular interaction becomes important. The potential well of 0.03 eV is deep enough to support many bound states of the $I_2 + I_2$ complex, and exceeds kT at room temperature or below. The same field exerts a significant degree of alignment on the molecule [17]. Consequently, we can speculate that cold molecules trapped in the laser focus may form linear van der Waals–type chains. If this were the case, the R^{-3} dependence of the attractive laser-induced interaction between the two molecules will be replaced by the stronger R^{-2} attraction in the chain.

Trapping reactants in laser-induced van der Waals–like minima may open a possibility for a *reaction path spectroscopy*, where transitions between vibrational levels of bound states along the reaction coordinate can be observed. As used here, ''reaction path spectroscopy'' would differ from the term ''transition state spectroscopy'' coined by Polanyi and co-workers [45] to describe electronic transitions along the reaction coordinate, as the latter makes no reference to the possibility of transitions between bound states on the lower surface. However, in that context the existence of bound states along the reaction path would necessarily increase the intensity of transitions to an upper electronic surface and thus make transition state spectra easier to observe. Such bound states will have a fluctuating well depth dependent on the laser intensity and frequency. Experimentally, a second probe laser will be needed in order to attempt to observe these bound states.

ACKNOWLEDGMENTS

The authors wish to thank A. Stolow, P. Corkum, and T. Seideman for helpful and inspiring discussions. M.I. acknowledges financial support from an NSERC (Canada) research grant to J.S.W. and partial financial support from an NSERC special collaborative research grant.

[1] See, e.g., M. Shapiro and Y. Zeiri, J. Chem. Phys. **85**, 6449 (1986); M. Shapiro and P. Brumer, *ibid.* **98**, 201 (1993); S. Shi and H. Rabitz, *ibid.* **92**, 364 (1990); J. Botina, H. Rabitz, and N. Rahman, *ibid.* **102**, 226 (1995); T. Seideman, M. Shapiro,and P. Brumer, *ibid.* **90**, 7132 (1989); P. Brumer and M. Shapiro, Acc. Chem. Res. **22**, 407 (1989).

[2] *Molecules in Laser Fields*, edited by A. Bandrauk (Marcel Dekker, New York, 1994).

[3] T. T. Nguyen-Dang and A. D. Bandrauk, J. Chem. Phys. **79**, 3256 (1983); **80**, 4926 (1984).

[4] P. H. Bucksbaum, A. Zavriev, H. G. Muller, and D. W. Schumacher, Phys. Rev. Lett. **64**, 1883 (1990); A. Zavriev, P. H. Bucksbaum, H. G. Muller, and D. W. Schumacher, Phys. Rev. A **42**, 5500 (1990).

[5] M. V. Fedorov, O. V. Kudrevatova, V. P. Makarov, and A. A. Samokhin, Opt. Commun. **13**, 299 (1975); A. D. Bandrauk and M. L. Sink, J. Chem. Phys. **74**, 1110 (1981); Chem. Phys. Lett. **57**, 569 (1978); J. F. McCann and A. D. Bandrauk, J. Chem. Phys. **96**, 903 (1992); A. Giusti-Suzor, X. He, O. Atabek, and F. H. Mies, Phys. Rev. Lett. **64**, 515 (1990); A. Giusti-Suzor and F. H. Mies, *ibid.* **68**, 3869 (1992).

[6] T. F. George, J. Phys. Chem. **86**, 10 (1982), and references therein.

[7] J. C. Light and A. Altenberger-Siczek, J. Chem. Phys. **70**, 4108 (1979).

[8] A. E. Orel and W. H. Miller, J. Chem. Phys. **73**, 241 (1980).

[9] T. Seideman and M. Shapiro, J. Chem. Phys. **88**, 5525 (1988); **94**, 7910 (1991).

[10] A. E. Orel and W. H. Miller, Chem. Phys. Lett. **57**, 362 (1978); J. Chem. Phys. **70**, 4393 (1979).

[11] R. D. Taylor and P. Brumer, J. Chem. Phys. **77**, 854 (1982).

[12] E. Charron, A. Giusti-Suzor, and F. H. Mies, Phys. Rev. Lett. **75**, 2815 (1995); **71**, 692 (1993).

[13] P. Dietrich and P. B. Corkum, J. Chem. Phys. **97**, 3187 (1992).

[14] M. Thachuk and D. Wardlaw, J. Chem. Phys. **102**, 7462 (1995).

[15] T. Seideman, M. Yu. Ivanov, and P. B. Corkum, Phys. Rev. Lett. **75**, 2819 (1995).

[16] P. Dietrich *et al.*, Phys. Rev. Lett. (to be published).

[17] B. Friederich and D. R. Herschbach, Phys. Rev. Lett. **74**, 4623 (1995).

[18] N. B. Delone and V. P. Krainov, *Multiphoton Processes in Atoms* (Springer-Verlag, Berlin, 1994).

[19] A. M. Perelomov, V. S. Popov, and M. V. Terent'ev, Zh. Éksp. Teor. Fiz. **50**, 1393 (1966) [Sov. Phys. JETP **23**, 924 (1966)]; M. V. Ammosov, N. B. Delone, and V. P. Krainov, *ibid.* **91**, 2008 (1986) [**64**, 1191 (1986)].

[20] P. B. Corkum, N. Burnett, and F. Brunel, Phys. Rev. Lett. **62**, 1259 (1989).

[21] S. L. Chin, Y. Liang, J. E. Decker, F. A. Ilkov, and M. V. Ammosov, J. Phys. B **25**, L249 (1992); T. Walsh, F. A. Ilkov, J. E. Decker, and S. L. Chin, *ibid.* **27**, 3767 (1994).

[22] F. A. Ilkov, T. Walsh, S. Turgeon, and S. L. Chin, Phys. Rev. A **51**, R2695 (1995); Chem. Phys. Lett. **247**, 1 (1995).

[23] K. M. Christoffel and J. M. Bowman, J. Phys. Chem. **85**, 2159 (1981); R. Walker and R. Preston, J. Chem Phys. **67**, 2017 (1977); A.D. Bandrauk and M. L. Sink, *ibid.* **74**, 1110 (1981); D. Permann and I. Hamilton, *ibid.* **97**, 3865 (1992); M. Tung and J.-M. Yuan, Phys. Rev. A **36**, 4463 (1987); J. Ackerhalt and P. Milonni, *ibid.* **37**, 1552 (1988); M. E. Goggin and P. Milonni, *ibid.* **37**, 796 (1988); **38**, 5174 (1988); R. Graham and M. Honnerbach, *ibid.* **43**, 3966 (1992); Z.-M. Lu, M. Vallieres, and J.-M. Yuan, *ibid.* **45**, 5512 (1992).

[24] W.-K. Liu, B. Wu, and J.-M. Yuan, Phys. Rev. Lett. **75**, 1292 (1995); S. Chelkowski, A.D. Bandrauk, and P. B. Corkum, *ibid.* **65**, 2355 (1990); S. Chelkowski and A.D. Bandrauk, Phys. Rev. A **41**, 6480 (1990).

[25] M. Yu. Ivanov, D. R. Matusek, and J. S. Wright, Chem. Phys. Lett. **255**, 232 (1996).

[26] M. Yu. Ivanov, D. R. Matusek, and J. S. Wright, Chem. Phys. Lett. **258**, 255 (1996).

[27] T. Zuo and A. Bandrauk, Phys. Rev. A **52**, R2511 (1995).

[28] P. Corkum, Phys. Rev. Lett. **71**, 1994 (1993).

[29] Y. Gontier and M. Trahin, Phys. Rev. A **40**, 1351 (1989).

[30] L. D. Landau and E. M. Lifshitz, *Classical Mechanics* (Pergamon Press, Oxford, 1960).

[31] R. A. Marcus, J. Chem. Phys. **45**, 4500 (1966).

[32] J. P. Heritage, A. M. Weiner, and R. N. Thurston, Opt. Lett. **10**, 609 (1985); **11**, 153 (1986); C. P. Huang *et al.*, *ibid.* **17**, 1289 (1992); J. Zhou *et al.*, *ibid.* **19**, 126 (1994).

[33] D. G. Truhlar and C. J. Horowitz, J. Chem. Phys. **68**, 2466 (1978); B. Liu, *ibid.* **58**, 1925 (1973); P. Siegbahn and B. Liu, *ibid.* **68**, 2457 (1978).

[34] K.P. Huber and G. Herzberg, *Molecular Spectra and Molecular Structure IV: Constants of Diatomic Molecules* (Van Nostrand Reinhold, New York, 1979).

[35] A. M. Frisch *et al.*, GAUSSIAN 92 (revision D.2), Gaussian Inc., Pittsburgh, PA, 1992.

[36] B. T. Ulrich, L. Ford, and J. C. Browne, J. Chem. Phys. **57**, 2906 (1972).

[37] Z. Peng, S. Kristyan, A. Kuppermann, and J. S. Wright, Phys. Rev. A **52**, 1005 (1995).

[38] P. A. Hyams, J. Gerratt, D. L. Cooper, and M. Raimondi, J. Chem. Phys. **100**, 4417 (1994).

[39] M. G. Papadopoulos, J. Waite, and A. D. Buckingham, J. Chem. Phys. **102**, 371 (1995).

[40] J. Rychlewski, Mol. Phys. **41**, 833 (1980).

[41] J. S. Wright, K. G. Tan, and K. J. Laidler, J. Chem. Phys. **64**, 970 (1976).

[42] F. T. Wall, L. A. Hiller, and J. Zazur, J. Chem. Phys. **29**, 255 (1958).

[43] H. R. Mayne, J. Chem. Phys. **73**, 217 (1980).

[44] J. S. Wright and K. G. Tan, J. Chem. Phys. **66**, 104 (1977); J. S. Wright, *ibid.* **69**, 720 (1978).

[45] H. R. Mayne, R. A. Poirier, and J. C. Polanyi, J. Chem. Phys. **80**, 4025 (1984).